Whistler turbulence forward cascade: Three-dimensional particle-in-cell simulations

Ouliang Chang

Department of Astronautical Engineering, University of Southern California, Los Angeles, California

S. Peter Gary

Los Alamos National Laboratory, Los Alamos, New Mexico

Joseph Wang

Department of Astronautical Engineering, University of Southern California, Los Angeles, California

---

Ouliang Chang and Joseph Wang, Department of Astronautical Engineering, University of Southern California, Los Angeles, CA. (e-mail: ouliang@usc.edu, josephjw@usc.edu)

S. Peter Gary, Los Alamos National Laboratory, Los Alamos, NM 87545. (e-mail: pgary@lanl.gov)

The first fully three-dimensional particle-in-cell (PIC) simulation of whistler turbulence in a magnetized, homogeneous, collisionless plasma has been carried out. An initial relatively isotropic spectrum of long-wavelength whistlers is imposed upon the system, with an initial electron β = 0.10. As in previous two-dimensional simulations of whistler turbulence, the three-dimensional system exhibits a forward cascade to shorter wavelengths and broadband, turbulent spectra with a wavevector anisotropy in the sense of stronger fluctuation energy at $k_\perp$ than at comparable $k_\parallel$ where the respective subscripts represent directions perpendicular and parallel to the background magnetic field $\mathbf{B}_o$. However, the three-dimensional (3D) simulations display quantitative differences with comparable two-dimensional (2D) computations. In the 3D runs, turbulence develops a stronger anisotropic cascade more rapidly than in 2D runs. Futhermore, reduced magnetic fluctuation spectra in 3D runs are less steep functions of perpendicular wavenumbers than those from 2D simulations. The much larger volume of perpendicular wavevector space in 3D appears to facilitate the transfer of fluctuation energy toward perpendicular directions.

1. Introduction

Historically, the primary focus for the study of plasma turbulence in the solar wind has been on the inertial range at observed frequencies $f \lesssim 0.2$ Hz [e.g., *Horbury et al.*, 2005; *Matthaeus and Velli*, 2011]. In this regime, magnetic fluctuation energy spectra exhibit dependences on frequency of the form $|\delta \mathbf{B}(f)|^2 \sim (f)^{-\alpha_f}$ with $\alpha_f \simeq 5/3$ and a strong characteristic wavevector anisotropy with greater fluctuation energy at propagation quasi-perpendicular to $\mathbf{B}_o$, the average background magnetic field, than at quasi-parallel propagation. At a frequency near 0.2 Hz $\lesssim f \lesssim$ 0.5 Hz, measurements at 1 AU show a spectral break, a distinct change to spectra that are steeper than those of the inertial range [*Leamon et al.*, 1998; *Smith et al.*, 2006; *Alexandrova et al.*, 2008]. At observed frequencies above this break, magnetic spectra exhibit steeper power laws, i.e., with 2.0 $\lesssim \alpha_f$ [*Behannon*, 1978; *Denskat et al.*, 1983; *Goldstein et al.*, 1994; *Lengyel-Frey et al.*, 1996; *Bale et al.*, 2005]. Recent analyses of data from the Cluster mission spacecraft have shown that magnetic spectra in the range 0.5 Hz $\lesssim f \lesssim$ 20 Hz scale with 2.6 $\lesssim \alpha_f \lesssim$ 2.8 [*Sahraoui et al.*, 2009, 2010; *Kiyani et al.*, 2009; *Alexandrova et al.*, 2009], and suggest that there is a second break with still more steeply decreasing spectra at 20 Hz $< f$. Some of these observations (*Chen et al.*, 2010; *Sahraoui et al.*, 2010) also demonstrated that this turbulence is anisotropic in the sense of having more fluctuation energy at propagation perpendicular to $\mathbf{B}_o$, where $\mathbf{B}_o$ denotes an average, uniform background magnetic field, than at propagation parallel or antiparallel to $\mathbf{B}_o$.

High frequency turbulence above the first spectral break is of small amplitude ($|\delta \mathbf{B}|^2 << B_o^2$), so that such turbulence is often described as being an ensemble of normal modes of the plasma with properties derived from linear dispersion theory. In this framework, there are two competing hypotheses as to the character of these fluctuations. One scenario is that this short-wavelength turbulence consists of kinetic Alfvén waves which propagate in directions quasi-perpendicular to $\mathbf{B}_o$ and at real frequencies $\omega_r < \Omega_p$, the proton cyclotron frequency. Both solar wind observations [*Leamon et al.*, 1998; *Bale et al.*, 2005; *Sahraoui et al.*, 2009, 2010] and gyrokinetic simulations [*Howes et al.*, 2008a, 2011; see also *Matthaeus et al.*, 2008, and *Howes et al.*, 2008c] of turbulence above the first break have been interpreted as consisting of kinetic Alfvén waves, although others have indicated that such fluctuations do not necessarily provide a complete description of short wavelength turbulence [*Gary and Smith*, 2009; *Podesta et al.*, 2010; *Chen et al.*, 2010]. A fluid model of kinetic Alfvén turbulence, which does not include kinetic plasma effects, yields magnetic fluctuation energy spectra which scale as $k_\perp^{-7/3}$, while inclusion of kinetic effects leads to still steeper spectra [*Howes et al.*, 2008b]. A recent three-dimensional gyrokinetic simulation of kinetic Alfvén turbulence has exhibited a $k_\perp^{-2.8}$ magnetic fluctuation spectrum [*Howes et al.*, 2011].

A second hypothesis is that whistler fluctuations at frequencies below the electron cyclotron frequency contribute to short-wavelength turbulence. Whistlers are often observed in the solar wind [*Beinroth and Neubauer*, 1981; *Lengyel-Frey et al.*, 1996]. Simulations of whistler turbulence using three-dimensional electron magnetohydrodynamic (EMHD) fluid models [*Biskamp et al.*, 1999; *Cho and Lazarian*, 2004, 2009; *Shaikh*, 2009] typically show a forward cascade to steep magnetic spectra with $k^{-7/3}$, and anisotropies similar to those of the inertial range with greater fluctuation energy at quasi-perpendicular propagation. Two-dimensional particle-in-cell (PIC) simulations of whistler turbulence [*Gary et al.*, 2008, 2010; *Saito et al.*, 2008, 2010; *Svidzinski et al.*, 2009], which include full kinetic effects such as Landau and cyclotron wave-particle interactions, also demonstrate forward cascades to anisotropic magnetic spectra with very steep wavenumber dependences (e.g., $k_\perp^{-4}$). Here we describe the first PIC simulations to examine the forward cascade of whistler turbulence in a fully three-dimensional plasma model.

Our simulation results are derived from a three-dimensional electromagentic particle-in-cell code 3D EMPIC described by *Wang et al.* [1995]. In this code, plasma particles are pushed using a standard relativistic particle algorithm; currents are deposited using a rigorous charge conservation scheme [*Villasenor and Buneman*, 1992]; and the self-consistent electromagnetic field is solved using a local finite difference time domain solution to the full Maxwell's equations. This code was recently modified and updated for this work. Specifically, the parallel computing part of the code has been optimized for hybrid parallel implementation to perform multithreading on clusters with multicore-processors. Space-filling curves are used in sorting particle array to preserve nearest-neighbor cells' proximity in memory. Such spatial proximity would enhance data locality, reduce cache miss, and thus further speed up the code. Our 3D simulations are performed at USC's HPC and NASA's Pleiades supercomputer systems. The upgraded 3D EMPIC code scales extremely well, with over 96% parallel efficiency on 2048 cores. The typical wall time of 3D runs is around 16 $\sim$ 17 hours.

We denote the jth species plasma frequency as $\omega_j \equiv \sqrt{4\pi n_j e_j^2/m_j}$, the jth species cyclotron frequency as $\Omega_j \equiv e_j B_o/m_j c$, and $\beta_{||j} \equiv 8\pi n_j k_B T_{||j}/B_o^2$. We consider an electron-proton plasma where subscript e denotes electrons and p stands for protons.

Here "three-dimensional" means that the simulation includes variations in three spatial dimensions, as well as calculating the full three-dimensional velocity space response of each ion and electron superparticle. The plasma is homogeneous with periodic boundary conditions. The uniform background magnetic field is $\mathbf{B}_o = \hat{\mathbf{z}} B_o$ so that the subscripts z and $||$ represent the same direction. Thus $\mathbf{k} = \hat{\mathbf{x}} k_x + \hat{\mathbf{y}} k_y + \hat{\mathbf{z}} k_{||}$ and $k_\perp = \sqrt{k_x^2 + k_y^2}$. We define two-dimensional reduced energy spectra by summation over the third Cartesian wavevector component, e.g.,

$$|\delta\mathbf{B}(k_x, k_y)|^2 \equiv \Sigma_{k_z} |\delta\mathbf{B}(\mathbf{k})|^2 \quad .$$

Similarly, one-dimensional reduced spectra for $k_{||}$ are obtained by summation over the two perpendicular wavevector components:

$$|\delta\mathbf{B}(k_{||})|^2 \equiv \Sigma_{k_x, k_y} |\delta\mathbf{B}(\mathbf{k})|^2 \quad .$$

In contrast, the one-dimensional reduced spectra for $k_\perp$ are obtained by summing the energy over both $k_{||}$ and concentric annular regions in k_x-k_y space. The total fluctuating magnetic energy density is obtained by summing over all simulation wavevectors:

$$|\delta\mathbf{B}|^2 \equiv \Sigma_{\mathbf{k}} |\delta\mathbf{B}(\mathbf{k})|^2$$

and the spectral anisotropy angle θ_B is defined via

$$\tan^2\theta_B \equiv \frac{\Sigma_{\mathbf{k}}\; k_\perp^2 |\delta\mathbf{B}(\mathbf{k})|^2}{\Sigma_{\mathbf{k}}\; k_{||}^2 |\delta\mathbf{B}(\mathbf{k})|^2} \quad .$$

An isotropic spectrum corresponds to $\tan^2 \theta_B$ =1.0. In the evaluation of each of these quantities, the wavenumber range of the summations is over the cascaded fluctuations; i.e., $0.55 \leq |kc/\omega_e| \leq 3.0$.

2. Simulations

This section describes results from three PIC simulations of the forward cascade of freely decaying whistler turbulence. For all three runs, as in *Gary et al.* [2008] and *Saito et al.* [2008], the grid spacing is $\Delta = 0.10c/\omega_e$, where c/ω_e is the electron inertial length, the time step is $\delta t\ \omega_e = 0.05$ and the number of superparticles per cell is 64. The system has a spatial length of $51.2c/\omega_e$ in each direction. For these parameters, the fundamental mode of all three simulations has wavenumber $kc/\omega_e = 0.1227$, and short wavelength fluctuations should be resolved up to the component wavenumber of $k_{||}c/\omega = k_{\perp}c/\omega_e = 4$. As in the two-dimensional simulations of *Saito et al.* [2008] and *Gary et al.* [2008, 2010], the initial physical dimensionless parameters are $m_p/m_e = 1836$, $T_e/T_p = 1.0$, $\beta_e = 0.10$, and $\omega_e^2/\Omega_e^2 = 5.0$.

We impose a three-dimensional spectrum of right-hand polarized whistler waves at $t = 0$. Initial wavenumbers parallel to $\mathbf{B}_o$ are $k_{||}c/\omega_e = \pm\ 0.1227$, $\pm\ 0.2454$, and $\pm\ 0.3682$, whereas initial perpendicular wavenumbers are the six same values and $k_{\perp}c/\omega_e = 0$. Different runs have different number (N) of modes imposed in the system, however, the initial total fluctuating magnetic field energy density is the same for all three runs: $\sum_{n=1}^{N} |\delta\mathbf{B}_n(t = 0)|^2/B_o^2 = 0.10$. The method of loading such an initial spectrum is described in *Saito et al.* [2008]. The frequencies and relationships among the field components are derived from the linear dispersion equation for magnetosonic-whistler fluctuations in a collisionless plasma, but the subsequent evolution of the fields and particles are computed using the fully nonlinear particle-in-cell simulation code.

Run 1 is a two-dimensional simulation with an initial spectrum similar to the corresponding runs of *Gary et al.* [2008] and *Saito et al.* [2008]. The domain size is 512×512 cells, which is equivalent to $51.2c/\omega_e \times 51.2c/\omega_e$. In this case, 42 modes are present in the y-z plane of the initial whistler spectrum. Runs 2 and 3 are three-dimensional simulations in which the system has a domain size of $512 \times 512 \times 512$ cells and spatial dimensions $L_x = L_y = L_z = 51.2c/\omega_e$. The only difference between these two runs is in the initial spectra. Run 2 has 42 modes in the y-z plane and 36 modes in the x-z plane (omitting the 6 modes at $k_\perp = 0$), whereas Run 3 has the same 78 modes as Run 2, but an additional 72 modes corresponding to a rotation of the Run 2 modes through an angle of 45^o about the z-axis. Figure 1 illustrates the distribution of the initial modes for the two three-dimensional cases. All three runs are computed to a final time of $|\Omega_e|t$ =447. The total particle plus fluctuating field energy of the system is conserved to within 0.6% between $t = 0$ and the final time.

Figure 2 shows two-dimensional reduced magnetic energy spectra from the three simulations at the final time. As in the two dimensional Run 1, the imposition of an initial spectrum of relatively long-wavelength whistlers in the three-dimensional runs leads to a forward cascade to shorter wavelengths and the development of a broadband, turbulent spectrum. The late-time spectrum in the k_x-k_y plane perpendicular to $\mathbf{B}_o$ is approximately gyrotropic, which is a consistency check on our homogeneous plasma simulation with initial conditions which are symmetric between x and y. The late-time reduced spectra in the two planes (k_x-k_z, k_y-k_z) containing $\mathbf{B}_o$ in all three runs show, just as in the two-dimensional PIC simulations of whistler turbulence [*Gary et al.*, 2008, 2010; *Saito et al.*, 2008, 2010], that the forward cascade is anisotropic, preferentially transfering energy to fluctuations with wavevectors quasi-perpendicular, rather than quasi-parallel, to $\mathbf{B}_o$.

The reduced magnetic k_y spectrum from the two-dimensional Run 1 at $|\Omega_e|t = 447$ is proportional to $k_y^{-4.0}$ over $0.25 \lesssim k_y c/\omega_e \lesssim 1.60$ (not shown), similar to the $k_y^{-4.5}$ late-time results for the two-dimensional simulations with $\epsilon = 0.10$ and initial $\beta_e = 0.10$ of *Gary et al.* [2008] and *Saito et al.* [2008]. Figure 3 illustrates the reduced $k_\perp$ spectra from the three-dimensional Runs 2 and 3 at $|\Omega_e|t = 447$. The results for the two runs are very similar, indicating that the late-time spectra are relatively independent of the detailed choice of initial fluctuations. The reduced spectra at relatively long wavelengths ($0.36 \lesssim k_\perp c/\omega_e \lesssim 1.0$) suggest a $k_\perp^{-3.1}$ dependence, whereas at shorter wavelengths ($1.0 \lesssim k_\perp c/\omega_e \lesssim 2.5$) the spectra become steeper with a $k_\perp^{-4.3}$ dependence. The upturn in the spectra at $k_\perp c/\omega_e \simeq 2.5$ corresponds to the noise level of the simulation. The suggestion of two distinct power-law regimes of the turbulence is similar to the prediction of *Meyrand and Galtier* [2010] who used an EMHD model with isotropic fluctuations to derive a $k^{-11/3}$ magnetic fluctuation spectrum at $1 < kc/\omega_e$. High-frequency turbulent spectra with breaks near the inverse electron inertial length have also been reported in the solar wind observations of *Sahraoui et al.* [2009, 2010] and *Alexandrova et al.* [2009].

Figure 4 compares the spectral anisotropies $\tan^2\theta_B$ of the three runs as functions of time. The results of the two-dimensional Run 1 are very similar to that of Run I from *Saito et al.* [2008], with $\tan^2\theta_B \sim 4$ at $|\Omega_e|t \simeq 400$. Both three-dimensional runs exhibit stronger anisotropies, with Run 2 reaching $\tan^2\theta_B \simeq 6$ and Run 3 attaining $\tan^2\theta_B > 10$ at late times. Our interpretation of these results is that the much larger number of quasi-perpendicular modes available in the three-dimensional cases allows the nonlinear wave-wave interactions and perpendicular cascades to proceed much more efficiently than in two dimensions. The successively increasing number of modes with $k_\perp$ components among these three runs implies more channels for perpendicular cascading and therefore a successively faster rate of such energy transfer for the fluctuations. Limits on our computational resources prevent us from continuing to move toward more dense modes in wavevector space, but the trend of these three runs indicates that such a condition should correspond to a highly anisotropic late-time condition with $\tan^2\theta_B >> 1$.

Figure 5(a) shows the total fluctuating magnetic field energy density as a function of time. Results of all three runs are qualitatively similar, demonstrating a gradual decrease of the total fluctuating magnetic field energy density. However, the three-dimensional simulations exhibit faster rates of fluctuation energy dissipation than the two-dimensional Run 1. Figure 5(b) shows that electrons have greater parallel kinetic energy gains in the three-dimensional runs than in the two-dimensional Run 1. The perpendicular energy gain of electrons is much weaker in all three runs, and there is no significant difference in this energy gain among the three cases.

Fig. 7 of *Saito et al.* [2008] shows that, at $k_\| c/\omega_e < 1$, the Landau resonance at oblique propagation is a stronger mechanism for whistler damping than the cyclotron resonance. Figure 4 shows that three-dimensional whistler turbulence (Runs 2 and 3) is more efficient at transferring fluctuation energy to oblique propagation than two-dimensional whistler turbulence (Run 1). This implies that, at such long wavelengths, 3D whistler turbulence is more efficient at dissipation than its two-dimensional counterpart. This provides a plausible explanation for the more rapid decrease of the fluctuating energy in the 3D simulations illustrated in Figure 5(a).

3. Conclusions

We have carried out the first fully three-dimensional particle-in-cell simulations of whistler turbulence in a homogeneous collisionless plasma with a uniform background magnetic field $\mathbf{B}_o$. We imposed an initial spectrum of relatively long-wavelength whistler fluctuations and computed the free decay of these modes to a broadband shorter wavelength regime of turbulence. This cascade yielded transfer of fluctuation energy to wavevectors preferentially quasi-perpendicular to $\mathbf{B}_o$. Both the forward cascade and its consequent wavevector anisotropy are qualitatively similar to previous results obtained from two-dimensional PIC simulations of whistler turbulence; quantitatively, however, the three-dimensional anisotropy develops faster and to a larger value than that in two-dimensional simulations. Furthermore, the more modes that are used as initial conditions, the more rapid the cascade and the more strongly anisotropic the turbulence becomes.

The reduced magnetic fluctuation energy spectrum of our two-dimensional simulation shows a $k_y^{-4.0}$ dependence at $k_y c/\omega_e \lesssim 1$, similar to the steep power-law behavior exhibited in earlier such simulations [*Saito et al.*, 2008, 2010]. In contrast, our three-dimensional simulations of Runs 2 and 3 show a less steep reduced spectrum of $k_\perp^{-3.1}$ at $k_\perp c/\omega_e \lesssim 1$, a spectral break near $k_\perp c/\omega_e \simeq 1$, and a steeper spectrum with $k_\perp^{-4.3}$ at shorter wavelengths, similar to recent observations of short-wavelength turbulence in the solar wind. Further three-dimensional simulations of whistler turbulence at different values of β_e and initial fluctuation amplitude must be carried out before more conclusions concerning whistler turbulence are reached.

Solar wind observations typically show $\beta_e \sim 1$, at which values electron Landau damping is strong and competes with wave-wave cascade processes. We have here used $\beta_e = 0.10$ to reduce Landau damping and to permit our simulations to isolate the consequences of wave-wave interactions. A complete study of whistler turbulence should address the high-β regime as well, but is beyond the purview of this work.

Acknowledgments. The authors acknowledge useful exchanges with Homa Karimabadi, Kaijun Liu, and Shinji Saito. We particularly appreciate extended discussions with John Podesta on the subject of computing magnetic spectral properties in three-dimensional models. The Los Alamos portion of this work was performed under the auspices of the U.S. Department of Energy (DOE). It was supported by the Solar and Heliospheric Physics SR&T and Heliophysics Guest Investigators Programs of the National Aeronautics and Space Administration, and by the joint DOE/National Science Foundation program in fundamental plasma research. The USC portion of this work was performed under an ONR MURI project led by the University of Maryland (Subaward Z882806). OC's research was also conducted as part of the Los Alamos Space Weather Summer School supported by the Institute of Geophysics and Planetary Physics, the Science, Technology and Engineering Directorate and the Global Security Directorate at Los Alamos National Laboratory. Computational resources supporting this work were provided by the USC High-Performance Computing and Communications (HPCC) as well as by the NASA

High-End Computing (HEC) Program through the NASA Advanced Supercomputing (NAS) Division at Ames Research Center.

References

Alexandrova, O., V. Carbone, P. Veltri, and L. Sorriso-Valvo (2008), Small-scale energy cascade of the solar wind turbulence, *Astrophys. J., 674*, 1153.

Alexandrova, O., J. Saur, C. Lacombe, A. Mangeney, J. Mitchell, S. J. Schwartz, and P. Robert (2009), Universality of solar wind turbulent spectrum from MHD to electron scales, *Phys. Rev. Lett., 103*, 165003.

Bale, S. D., P. J. Kellogg, F. S. Mozer, T. S. Horbury, and H. Reme (2005), Measurement of the electric fluctuation spectrum of magnetohydrodynamic turbulence, *Phys. Rev. Lett., 94*, 215002.

Behannon, K. W. (1978), Heliocentric distance dependence of the interplanetary magnetic field, *Revs. Geophys.*, *16*, 125.

Beinroth, H. J., and F. M. Neubauer (1981), Properties of whistler mode waves between 0.3 and 1.0 AU from Helios observations, *J. Geophys. Res., 86*, 7755.

Biskamp, D., E. Schwarz, A. Zeiler, A. Celani, and J. F. Drake (1999), Electron magnetohydrodynamic turbulence, *Phys. Plasmas*, *6*, 751.

Cho, J., and A. Lazarian (2004), The anisotropy of electron magnetohydrodynamic turbulence, *Astrophys. J., 615*, L41.

Cho, J., and A. Lazarian (2009), Simulations of electron magnetohydrodynamic turbulence, *Astrophys. J., 701*, 236.

Chen, C. H. K., T. S. Horbury, A. A. Schekochihin, R. T. Wicks, O. Alexandrova, and J. Mitchell (2010), Anisotropy of solar wind turbulence in the dissipation range, *Phys. Rev. Lett., 104*, 255002.

Denskat, K. U., H. J. Beinroth, and F. M. Neubauer (1983), Interplanetary magnetic field power spectra with frequencies from 2.4 x 10^{-5} Hz to 470 Hz from HELIOS- observations during solar minimum conditions, *J. Geophys.*, *54*, 60.

Gary, S. P., and C. W. Smith (2009), Short-wavelength turbulence in the solar wind: Linear theory of whistler and kinetic Alfvén fluctuations, *J. Geophys. Res., 114*, A12105, doi:10.1029/2009JA014525.

Gary, S. P., S. Saito, and H. Li (2008), Cascade of whistler turbulence: Particle-in-cell simulations, *Geophys. Res. Lett., 35*, L02104, doi:10.1029/2007GL032327.

Gary, S. P., S. Saito, and Y. Narita (2010), Whistler turbulence wavevector anisotropies: Particle-in-cell simulations, *Astrophys. J., 716*, 1332.

Goldstein, M. L., D. A. Roberts, and C. A. Fitch (1994), Properties of the fluctuating magnetic helicity in the inertial and dissipation ranges of solar wind turbulence, *J. Geophys. Res., 99*, 11,519.

Horbury, T. S., M. A. Forman, and S. Oughton (2005), Spacecraft observations of solar wind turbulence: An overview, *Plasma Phys. Control. Fusion*, *47*, B703.

Howes, G. G., W. Dorland, S. C. Cowley, G. W. Hammett, E. Quataert, A. A. Schekochihin, and T. Tatsuno (2008a), Kinetic simulations of magnetized turbulence in astrophysical plasmas, *Phys. Rev. Lett., 100*, 065004.

Howes, G. G., S. C. Cowley, W. Dorland, G. W. Hammett, E. Quataert, and A. A. Schekochihin (2008b), A model of turbulence in magnetized plasmas: Implications for the dissipation range in the solar wind, *J. Geophys. Res., , 113*, A05103.

Howes, G. G., S. C. Cowley, W. Dorland, G. W. Hammett, E. Quataert, A. A. Schekochihin, and T. Tatsuno (2008c), Reply, *Phys. Rev. Lett., 101*, 149502.

Howes, G. G., J. M. TenBarge, W. Dorland, E. Quataert, A. A. Schekochihin, R. Numata, and T. Tatsuno (2011), Gyrokinetic simulations of solar wind turbulence from ion to electron scales, *Phys. Rev. Lett., 107*, 035004.

Kiyani, K. H., S. C. Chapman, Yu. V. Khotyaintsev, M. W. Dunlop, and F. Sahraoui (2009), Global scale-invariant dissipation in collisionless plasma turbulence, *Phys. Rev. Lett., 103*, 075006.

Leamon, R. J., C. W. Smith, N. F. Ness, W. H. Matthaeus, and H. K. Wong (1998), Observational constraints on the dynamics of the interplanetary magnetic field dissipation range, *J. Geophys. Res., 103*, 4775.

Lengyel-Frey, D., R. A. Hess, R. J. MacDowall, R. G. Stone, N. Lin, A. Balogh, and R. Forsyth (1996), Ulysses observations of whistler waves at interplanetary shocks and in the solar wind, *J. Geophys. Res., 101*, 27,555.

Matthaeus, W. H., S. Servidio, and P. Dmitruk (2008), Comment on "Kinetic simulations of magnetized turbulence in astrophysical plasmas," *Phys. Rev. Lett., 101*, 149501.

Matthaeus, W. H., and M. Velli (2011), Who needs turbulence? A review of turbulence effects in the heliosphere and on the fundamental process of reconnection, *Space Sci. Revs.*, doi 10.1007/s11214-011-9793-9.

Meyrand, R., and S. Galtier (2010), A universal law for solar-wind turbulence at electron scales, *Astrophys. J., 721*, 1421.

Podesta, J. J., J. E. Borovsky, and S. P. Gary (2010), A kinetic Alfvén wave cascade subject to collisionless damping cannot reach electron scales in the solar wind at 1 AU, *Astrophys. J., 712*, 685.

Sahraoui, F., M. L. Goldstein, P. Robert, and Yu. V. Khotyaintsev (2009), Evidence of a cascade and dissipation of solar-wind turbulence at the electron gyroscale, *Phys. Rev. Lett., 102*, 231102.

Sahraoui, F., M. L. Goldstein, G. Belmont, P. Canu, and L. Rezeau (2010), Three dimensional anisotropic k spectra of turbulence at subproton scales in the solar wind, *Phys. Rev. Lett., 105*, 131101.

Saito, S., S. P. Gary, H. Li, and Y. Narita (2008), Whistler turbulence: Particle-in-cell simulations, *Phys. Plasmas*, *15*, 102305.

Saito, S., S. P. Gary, and Y. Narita (2010), Wavenumber spectrum of whistler turbulence: Particle-in-cell simulation, *Phys. Plasmas*, *17*, 122316.

Shaikh, D. (2009), Whistler wave cascades in solar wind plasma, *Mon. Not. R. Astron. Soc.*, *395*, 2292.

Smith, C. W., K. Hamilton, B. J. Vasquez, and R. J. Leamon (2006), Dependence of the dissipation range spectrum of interplanetary magnetic fluctuations on the rate of energy cascade, *Astrophys. J., 645*, L85.

Svidzinski, V. A., H. Li, H. A. Rose, B. J. Albright, and K. J. Bowers (2009), Particle in cell simulations of fast magnetosonic wave turbulence in the ion cyclotron frequency range, *Phys. Plasmas*, *16*, 122310.

Villasenor, J., and O. Buneman (1992), Rigorous charge conservation for local electromagnetic field solvers, *Comput. Phys. Commun.*, *69*, 306.

Wang, J., P. Liewer, and V. Decyk (1995), 3D electromagnetic plasma particle simulations on a MIMD parallel computer, *Comput. Phys. Commun.*, *87*, 35.

Figure 1. Two-dimensional reduced magnetic fluctuation energy spectra at $t = 0$: (left panel) Run 2 in the plane perpendicular to $\mathbf{B}_o$, (center panel) Run 3 in the plane perpendicular to $\mathbf{B}_o$, and (right panel) Run 3 in the k_y-k_z plane containing $\mathbf{B}_o$.

Figure 2. Two-dimensional reduced magnetic fluctuation energy spectra at $|\Omega_e|t = 447$ from Run 1 (left panel), Run 2 (center panels) and Run 3 (right panels). The upper row of panels represents spectra in the k_y-k_z plane, whereas the bottom row of panels represents spectra in the plane perpendicular to $\mathbf{B}_o$.

Figure 3. Reduced $k_\perp$ magnetic fluctuation energy spectra at $|\Omega_e|t = 447$ from Run 2 and Run 3 (as labeled). The dashed lines represent power law functions as labeled for comparison against the simulation results.

Figure 4. Time histories of the spectral anisotropy factor $\tan^2\theta_B$ from the two-dimensional Run 1 (red line) and the three-dimensional Run 2 (green line) and Run 3 (blue line) simulations. Evaluations here are taken on spectra over $0.65 \leq kc/\omega_e \leq 3.0$.

Figure 5. Time histories of the (a) total fluctuating magnetic energy density and (b) the parallel (solid lines) and perpendicular (dashed lines) components of the total electron kinetic energy as functions of time. Here the red lines represent the two-dimensional Run 1 whereas the green and blue lines represent the three-dimensional Runs 2 and 3, respectively.

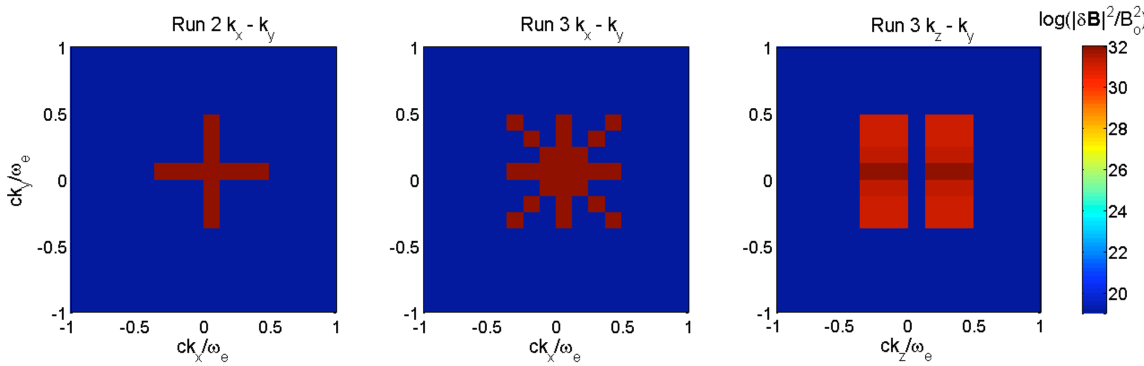

Figure 1

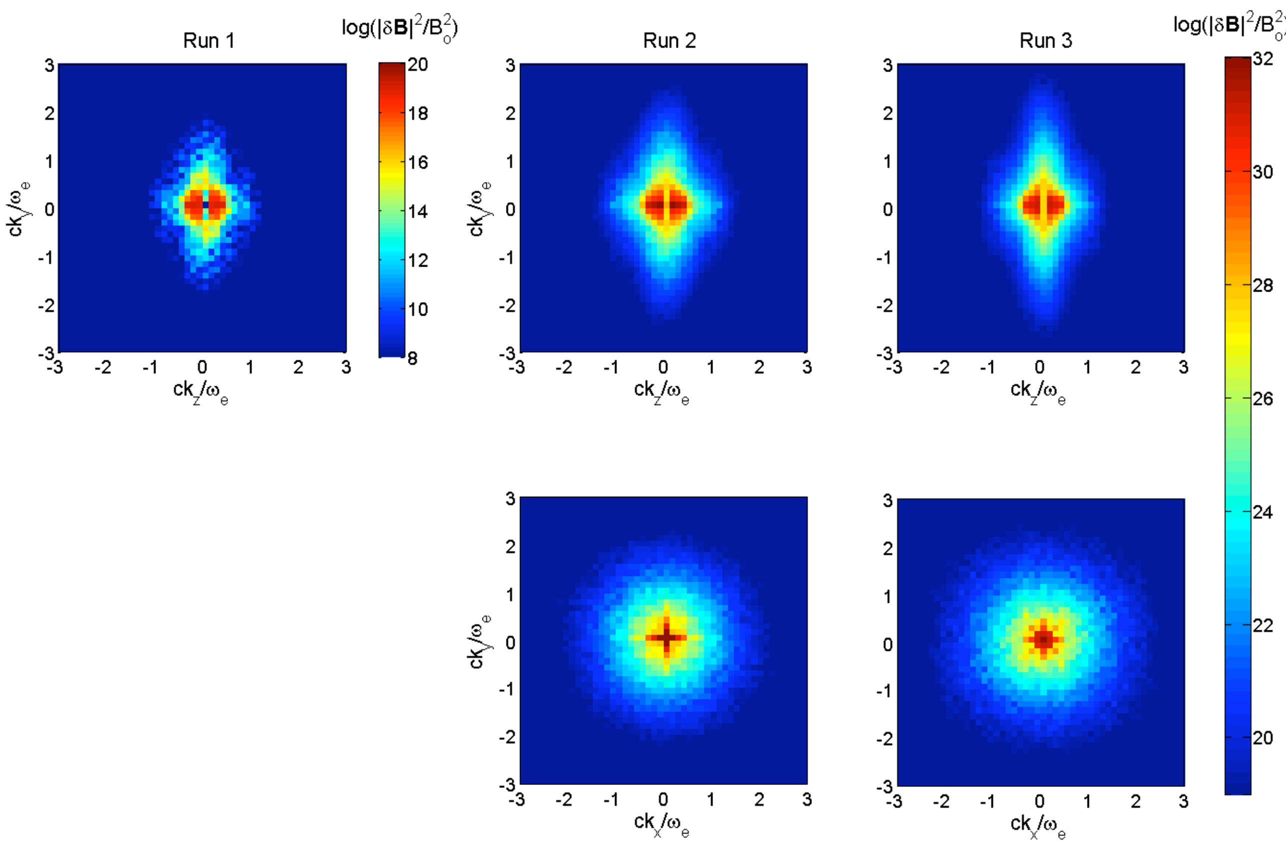

Figure 2

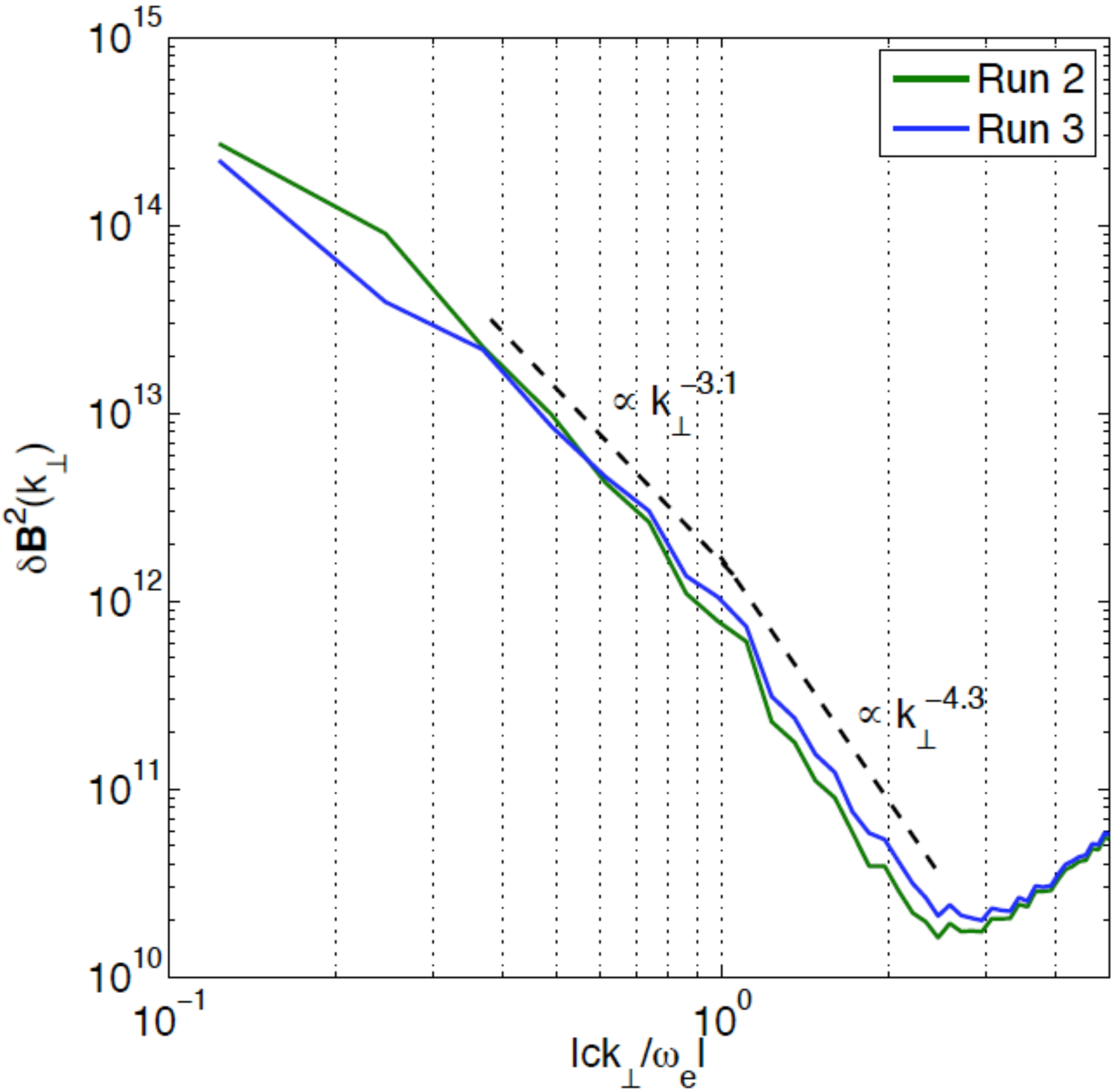
Run 2
Run 3
$\propto k_\perp^{-3.1}$
$\propto k_\perp^{-4.3}$
$\delta\mathbf{B}^2(k_\perp)$
$|ck_\perp/\omega_e|$
10^{15}
10^{14}
10^{13}
10^{12}
10^{11}
10^{10}
10^{-1}
10^{0}

Figure 3

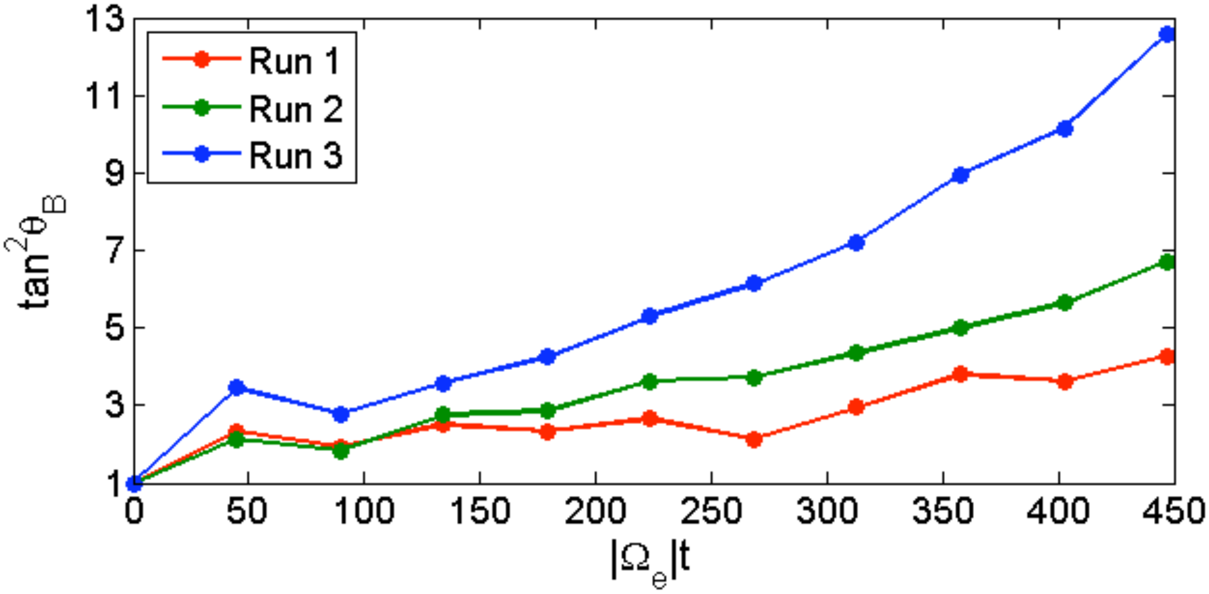

Run 1
Run 2
Run 3
$\tan^2\theta_B$
$|\Omega_e|t$
0
50
100
150
200
250
300
350
400
450
1
3
5
7
9
11
13

Figure 4

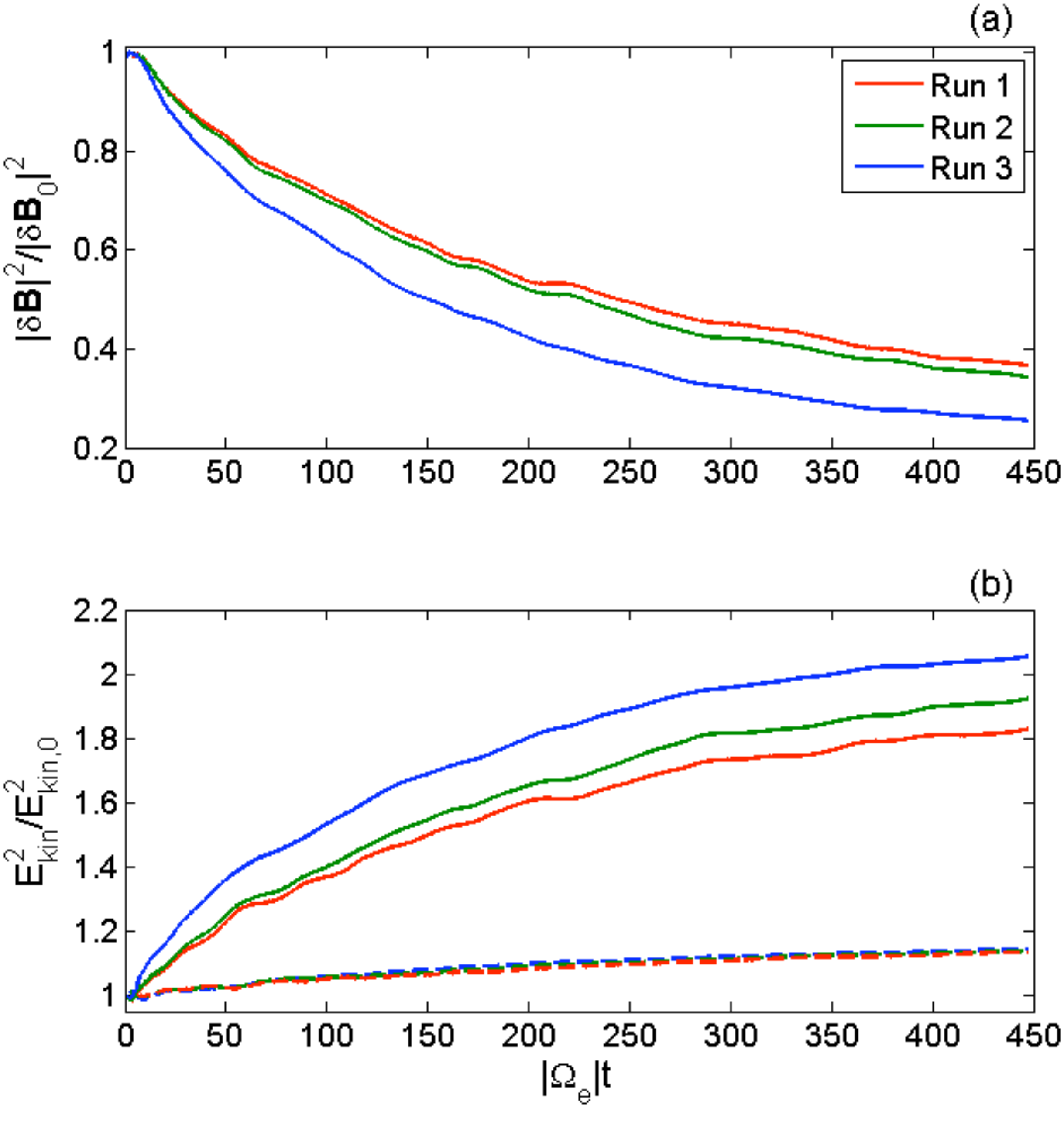

(a)
Run 1
Run 2
Run 3
$|\delta\mathbf{B}|^2/|\delta\mathbf{B}_0|^2$
0.2
0.4
0.6
0.8
1
0
50
100
150
200
250
300
350
400
450
(b)
$E^2_{kin}/E^2_{kin,0}$
1
1.2
1.4
1.6
1.8
2
2.2
$|\Omega_e|t$

Figure 5